Editors' Suggestion | Featured in Physics

Millisecond Coherence in a Superconducting Qubit

Aaron Somoroff,[1] Quentin Ficheux,[1] Raymond A. Mencia,[1] Haonan Xiong,[1] Roman Kuzmin,[1] and Vladimir E. Manucharyan[1,2]

[1]*Department of Physics, Joint Quantum Institute, and Quantum Materials Center, University of Maryland, College Park, Maryland 20742, USA*

[2]*École Polytechnique Fédérale de Lausanne, CH-1015 Lausanne, Switzerland*

(Received 21 April 2021; revised 24 March 2023; accepted 10 May 2023; published 29 June 2023)

Improving control over physical qubits is a crucial component of quantum computing research. Here we report a superconducting fluxonium qubit with *uncorrected* coherence time $T_2^* = 1.48 \pm 0.13$ ms, exceeding the state of the art for transmons by an order of magnitude. The average gate fidelity was benchmarked at 0.99991(1). Notably, even in the millisecond range, the coherence time is limited by material absorption and could be further improved with a more rigorous fabrication. Our demonstration may be useful for suppressing errors in the next generation quantum processors.

DOI: 10.1103/PhysRevLett.130.267001

Superconducting qubits have become a major quantum computing platform in large part because of a rapid growth of coherence time [1,2], beginning with the first demonstration of coherent oscillations in a Cooper pair box circuit in 1999 [3]. Notable leaps took place with the invention of quantronium [4] and 3D-transmon qubits [5], the latter leading to a widespread use of transmons and related circuits, such as X-mons [6] and C-shunt flux qubits [7]. However, despite promising recent developments [8], the coherence time of superconducting qubits, as measured using the conventional Ramsey interference protocol, has remained at about 100 μs for almost a decade [9]. The limited coherence of physical qubits slows down the implementation of useful noisy intermediate-scale quantum (NISQ) processors [10,11] and ultimately intensifies the hardware requirement for quantum error correction [12,13]. In this Letter, we present a case study of a superconducting qubit of the less explored fluxonium type [14], the uncorrected (Ramsey) coherence time of which robustly exceeded 1 msec.

Our circuit [see Figs. 1(a) and 1(b)] consists of a relatively weak Josephson junction (Josephson energy $E_J/h = 5.57$ GHz) connected to an antennalike capacitance and a compact large-value inductance (superinductance), realized with an array of about a hundred relatively strong junctions ($E_J/h = 106$ GHz). The circuit design is similar to that introduced in Refs. [15,16] except the substrate is changed from silicon to sapphire. Dynamics of fluxoniums can be described using a pair of conjugate operators $\hat{\varphi}$ and $\hat{n} = -i\partial_\varphi$, representing, respectively, the superconducting phase twist across the inductance and the charge displaced at the capacitor plates (in units of the Cooper pair charge). The chip is placed inside a copper cavity, with a resonance frequency of 7.54 GHz and a quality factor of $Q = 417$, in order to perform a dispersive readout of the qubit state [17]. A separate port in the cavity is used for wireless driving of the fluxonium transitions. The circuit parameters are accurately determined from spectroscopy data as a function of flux through the loop,

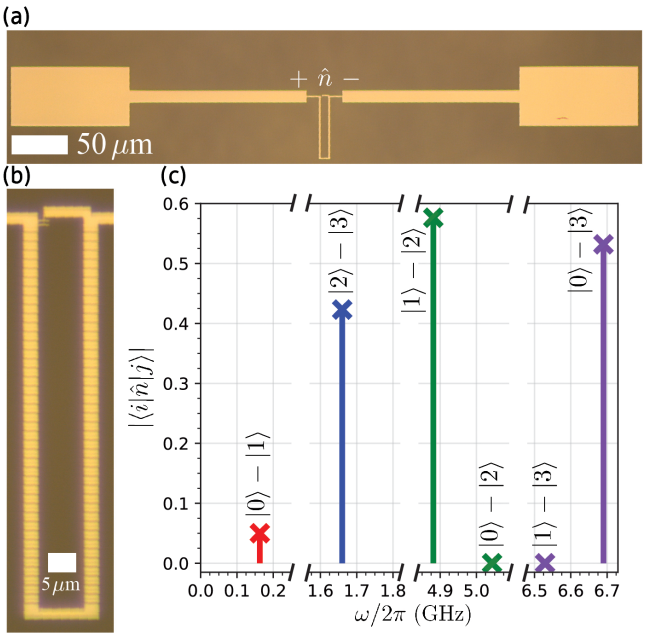

FIG. 1. (a) Optical image of the measured device. The antenna electrodes are attached directly to the weak junction of fluxonium, contributing to the total shunting capacitance and coupling the qubit to a copper box readout resonator (not shown). (b) Close up of the fluxonium loop formed by the weak junction (top left corner) and a chain of stronger junctions. (c) Measured frequencies and calculated charge operator $\hat{n}$ matrix elements for transitions between the lowest three energy levels at the half-integer flux bias. Note, the qubit transition $|0\rangle - |1\rangle$ is allowed, albeit suppressed in comparison to transition $|1\rangle - |2\rangle$, and transitions $|0\rangle - |2\rangle$ and $|1\rangle - |3\rangle$ are dipole forbidden.

which, along with the details of our experimental procedures, are available in the Supplemental Material [18].

At the half-integer flux bias, fluxoniums are practically unaffected by the background $1/f$ flux noise [15,19], thanks to the large value of the inductive shunt. The spectrum of relevant transitions in the present device is concisely summarized in Fig. 1(c). The qubit transition between the lowest energy states $|0\rangle$ and $|1\rangle$ has a frequency $\omega_{01}/2\pi = 163$ MHz. In comparison to transmons, such a qubit is better protected against energy relaxation into charge defects in the circuit material [20], because of the reduced matrix element $|\langle 0|\hat{n}|1\rangle| \ll 1$ (for transmons, $|\langle 0|\hat{n}|1\rangle| \sim 1$), and against uncontrolled leakage of quantum information into higher energy states, because of the extraordinary large anharmonicity. The noncomputational transitions $|1\rangle - |2\rangle$ and $|0\rangle - |3\rangle$ are instrumental to designing an on-demand qubit-qubit interaction [21], as they have much larger frequency and charge matrix elements. In fact, high-fidelity controlled-Z and controlled-phase gates on a pair of capacitively coupled fluxoniums with similar spectra to that shown in Fig. 1 have been recently demonstrated [22,23].

The qubit energy relaxation time T_1 is measured by applying a π pulse to the $|0\rangle - |1\rangle$ transition and reading out the excited state population after a variable time delay. Prior to the π pulse, the qubit is partially initialized using a cavity pulse in the high photon number regime (see Supplemental Material [18], note 2C). The coherence time T_2^* is obtained from the sequence of two $\pi/2$ pulses separated by a variable time delay. This protocol produces a Ramsey fringe oscillating at the drive-qubit detuning frequency $\Delta\nu$ and has an exponentially decaying envelope with a characteristic time T_2^*. The two pulse sequences were interleaved and repeated over a period of about 12 h. The fit values of T_1, T_2^* and $\Delta\nu$ are shown in Fig. 2(a). The highest recorded coherence time $T_2^* = 1.48 \pm 0.13$ ms exceeds the state of the art value for both transmons and fluxoniums by an order of magnitude. This coherence time is attainable thanks to the long average energy relaxation time $\bar{T}_1 = 1.20 \pm 0.03$ ms of our qubit. Averaging the Ramsey fringes measured over a period of 12 h results in only a minor reduction of the coherence time to $\bar{T}_2^* = 1.16 \pm 0.05$ ms [Fig. 2(b)]. Accordingly, the qubit frequency variation over the 12 h period is contained within a 100 Hz interval, much narrower than what is commonly reported [24]. Likewise, averaging the energy relaxation signal shows no signs of double-exponential behavior, typical to the case of a decay rate fluctuating in time [Fig. 2(c)]. In fact, the values of T_1 and T_2^* were stable around 1 ms over a period of several months.

Coherent control over a single qubit can be more rigorously characterized using the randomized benchmarking (RB) technique [25,26]. In a RB sequence, m randomly chosen Clifford gates are performed on the qubit before applying a single recovery gate, chosen to bring the state vector back to the initial state. The excited state probability $p(|1\rangle)$ decays with the sequence length m as $A + Bp^m$, where p is the depolarization parameter, and A, B are constants that absorb state preparation and measurement (SPAM) errors [see the red curve in Fig. 3(a)]. We extract an average error rate of a Clifford operation r_{cliff} given by $r_{\text{cliff}} = (1-p)/2 = (1.7 \pm 0.2) \times 10^{-4}$. Because each Clifford operation is composed on average of 1.833 physical gates (we do not count the identity gate), the average physical gate fidelity is given by $F = 1 - r_{\text{cliff}}/1.833 = 0.99991(1)$. To our knowledge, a significantly higher fidelity number has been possible only in trapped ion demonstrations [27].

The fidelity of each physical gate in the list $(\pm X, \pm Y, \pm X/2, \pm Y/2)$ can be extracted using an interleaved RB sequence: a given gate is interleaved between each Clifford operation. The resulting curve follows the same decay profile as the standard RB, but with a depolarization parameter p_g (see Supplemental Material [18], note 3). The physical gate error is given by $r_g = (1 - p_g/p)/2 = 1 - F_g$, where p is the depolarization parameter obtained from reference RB and F_g is the fidelity of the physical gate. The error rates of each physical

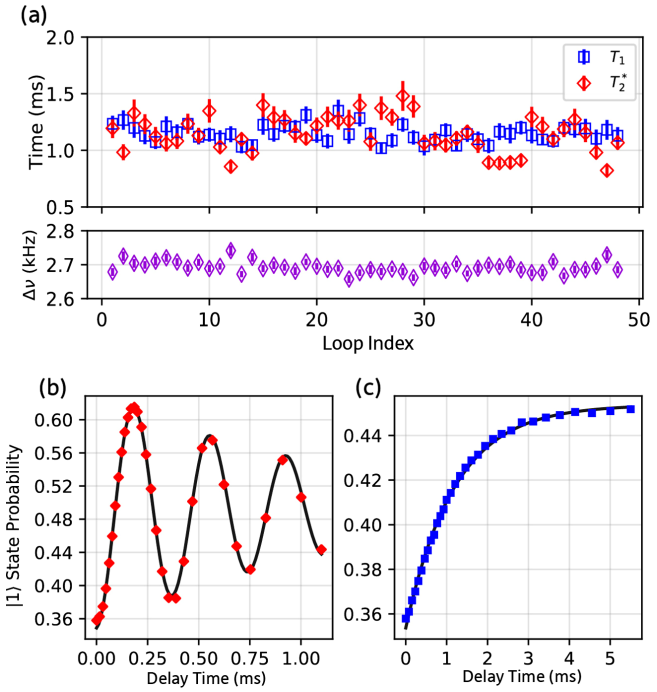

FIG. 2. (a) Ramsey coherence time T_2^* and energy relaxation time T_1, measured simultaneously and repeatedly over a period of 12 h. Lower panel shows the Ramsey fringe frequency $\Delta\nu$, the fluctuations of which are contained within 100 Hz. (b) Ramsey fringe data averaged over the entire 12-h period. The solid line is the fit to a decaying sinusoid with characteristic time $\bar{T}_2^* = 1.16 \pm 0.05$ ms. (c) Energy relaxation data averaged across the same 12-h period. The solid line is an exponential fit with a time constant $\bar{T}_1 = 1.20 \pm 0.03$ ms.

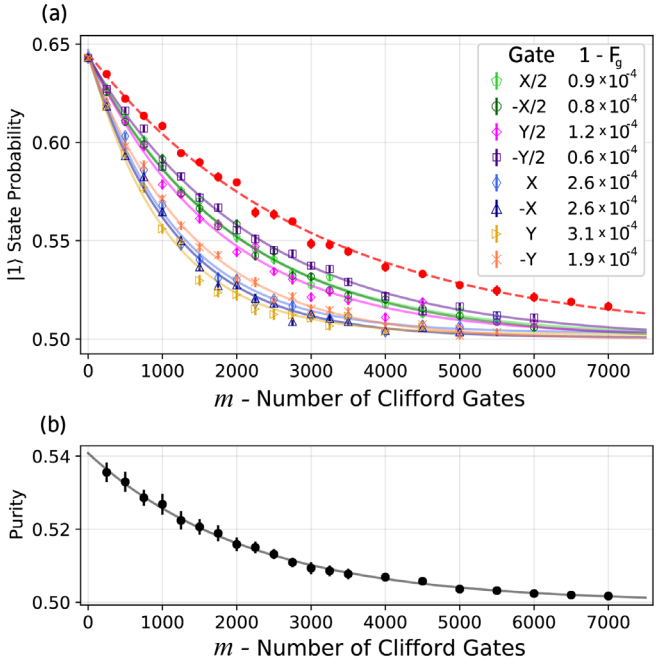

FIG. 3. (a) Results of randomized benchmarking (RB). The red curve (solid markers) is the reference RB sequence with an average Clifford gate error rate of $(1.7 \pm 0.2) \times 10^{-4}$, which converts to the average fidelity of the physical gates used to generate the Clifford group of 0.99991(1) (see text). The eight other curves are the interleaved RB sequences, where each color marks a given interleaved gate. The relative uncertainty on the gate errors given in the caption is about 10%. (b) Results of purity benchmarking. Solid markers indicate the purity of the quantum state versus number of Clifford gates. The decay rate coverts to the average error due to decoherence of 0.6×10^{-4}, establishing an upper bound on the achievable average gate fidelity of 0.99994.

gate, $1 - F_g$, are quoted in the inset of Fig. 3(a). Note that the average of the values F_g listed in Fig. 3(a) differs from the average physical gate fidelity F composing a Clifford operation, because there are more $\pi/2$ than π rotations, on average, in a Clifford operation. The decoherence contribution to the gate error can be estimated using the purity benchmarking (PB) procedure [28–30]. Purity benchmarking consists of performing state tomography of the qubit at the end of the RB sequence instead of the recovery gate. The purity $P = \mathrm{tr}(\rho^2)$ of the qubit state decays as $A' + B'u^{m-1}$ [see Fig. 3(b)], where u is called the unitarity and A', B' are constants. The error rate due to decoherence per Clifford gate is $r_{\mathrm{dec,cliff}} = (1 - \sqrt{u})/2 \simeq 1.1 \times 10^{-4}$, and the error rate due to decoherence per gate is $r_{\mathrm{dec,gate}} = r_{\mathrm{dec,cliff}}/1.833 \simeq 0.6 \times 10^{-4}$. We conclude that most of the gate error is caused by incoherent processes and hence can be reduced even further by shortening the pulses.

Having established exceptional figures on coherence and gate fidelity, we proceed with an in-depth characterization of our qubit device. To start, we use single-shot readout histograms (Supplemental Material [18], note 2A) to find the dispersive shift $\chi_{01}/2\pi = 1.16$ MHz. The quantity χ_{01} sets the qubit-cavity interaction rate in the dispersive limit and it is just as large as in a typical 3D-transmon-based cQED. The discrepancy between simultaneously measured values of $T_2 = 1.55$ ms (using a single echo π pulse) and $2T_1 = 2.1$ ms cannot be explained by dephasing due to $1/f$ flux noise, the magnitude of which is bounded by the data off the sweet spot [15]. However, it may be explained by the presence of approximately 4×10^{-4} photons, on average, in the cavity, given the known values of χ_{01} and κ (see Supplemental Material [18], note 2). Such a cavity occupation would correspond to a temperature of about 46 mK, which is larger than the base temperature of our dilution refrigerator (10 mK) but consistent with previous reports using heavy attenuation at the readout frequency [31–33]. We designed $\chi_{01}/\kappa \ll 1$ to limit thermal photon dephasing, which reduced the readout fidelity.

The single-shot readout histograms also provide an accurate value of the effective qubit temperature of 25 mK, extracted from fitting the equilibrium populations of states $|0\rangle$ and $|1\rangle$. This temperature value is a factor of 1.5–2 lower than what is typically measured in transmons, but here the qubit frequency is much lower as well. One may reasonably expect a frequency-dependent temperature for a qubit facing an out-of-equilibrium environment. We checked that raising the refrigerator temperature to 25 mK did not modify T_1 appreciably, but going to 50 mK increased the relaxation rate by a factor of 3, in agreement with the stimulated emission factor.

Next, we turn to characterizing the energy relaxation. Figure 4(a) shows the measurement of $T_1 \equiv T_1^{01}$ vs qubit frequency ω_{01}, obtained by tuning the flux away from the sweet spot. Each data point has been taken by applying a proper π pulse on resonance with the new qubit frequency, and we have manually checked that each relaxation trace was single-exponential. The data reveals *reproducible* fluctuations of T_1^{01} in frequency. These fluctuations qualitatively eliminate out-of-equilibrium quasiparticles as the dominant relaxation mechanism, and rather point at the absorption by material defects. Interestingly, neither the high nor the low values of T_1 in Fig. 4(a) show any trend for an increase towards the half-integer sweet-spot, which contrasts the observations reported in Ref. [34]. It is also worth noting that quantum defect spectroscopy has not been available so far in the sub-GHz frequency range (the T_1 data in Ref. [34] show fluctuations of T_1 in time rather than in frequency), which makes the data in Fig. 4(a) valuable for modeling dielectric loss mechanisms.

Finally, we introduce a new loss characterization experiment, which consists of measuring the rate $\Gamma_{02} \equiv 1/T_1^{02}$ of direct relaxation between states $|2\rangle$ and $|0\rangle$ [Fig. 4(b)]. This process should not be confused with a relatively fast indirect relaxation $|2\rangle \rightarrow |1\rangle$, which has a characteristic time $T_1^{12} \approx 10$–20 μs (Supplemental Material [18], note 6). Our protocol for measuring T_1^{02} is shown schematically in

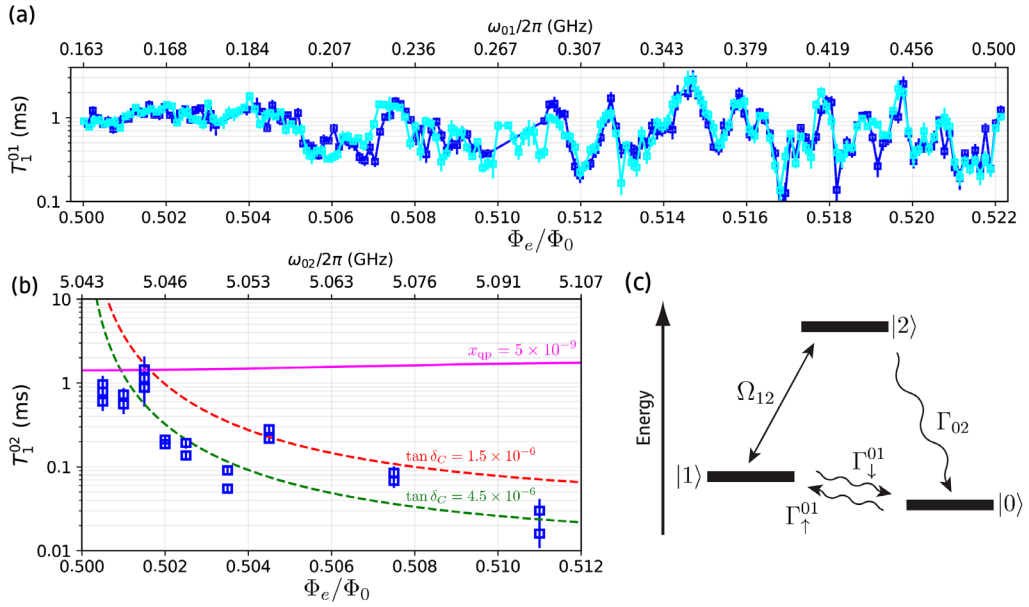

FIG. 4. (a) Energy relaxation time T_1^{01} of transition $|0\rangle - |1\rangle$ versus external magnetic flux Φ_e. Marker color indicates two separate scans taken 24 h apart. (b) Energy relaxation time T_1^{02} of transition $|0\rangle - |2\rangle$ versus flux. Red and green dashed curves represent the dielectric loss model with an effective loss tangent 1.5×10^{-6} and 4.5×10^{-6}, respectively. The magenta curve is the limit imposed by quasiparticle tunneling across the fluxonium's weak junction, characterized by an effective quasiparticle density $x_{qp} = 5 \times 10^{-9}$ (see text). (c) Schematic of the driving (straight arrow) and relaxation (wavy arrows) processes involved in measuring the relaxation rate $\Gamma_{02} \equiv 1/T_1^{02}$. Thermal occupation of state $|2\rangle$ is neglected. Details of the experimental procedure are provided in Supplemental Material [18], note 7.

Fig. 4(c). It requires a large ratio of $T_1^{01}/T_1^{12} \sim 10^2$, as well as an accurate calibration of the qubit temperature and lifetime T_1^{01} at every flux bias (Supplemental Material [18], note 7). Note that $T_1^{01} = 1/(\Gamma_\downarrow^{01} + \Gamma_\uparrow^{01})$, where $\Gamma_\downarrow^{01}$ and $\Gamma_\uparrow^{01}$ are the relaxation and excitation rates of the qubit transition, respectively. We apply a saturating Rabi drive for a given duration τ to the $|1\rangle - |2\rangle$ transition with Rabi frequency Ω_{12}, wait for a period of a few times T_1^{12}, and then record the population $p_0(\tau)$ of state $|0\rangle$. The deviation of p_0 from its equilibrium value indicates a direct transfer of population from state $|2\rangle$ to state $|0\rangle$. We model the quantity $p_0(\tau)$ using a three-level scheme and extract the value of T_1^{02} as the sole adjustable parameter.

The T_1^{02} data [Fig. 4(b)] is particularly useful as it involves relaxation processes at a frequency around $\omega_{02}/2\pi \approx 5$ GHz and hence allows for a more direct comparison to transmons. We find that T_1^{02} rapidly grows as the flux bias approaches the half-integer value, where transition $|0\rangle - |2\rangle$ is forbidden [Fig. 4(b)]. The data in Fig. 4(b) agree with a standard dielectric loss model assuming that the total capacitance C across the junction has a loss tangent $\tan\delta_C \approx (1.5\text{–}4.5) \times 10^{-6}$ (Supplemental Material [18], note 4). These values of $\tan\delta_C$ are consistent with our previous measurements [15] but are larger than those reported for transmons [20].

The most intriguing data point in Fig. 4(b) is the saturation of $T_1^{02} \approx 1.5$ ms at the half-integer flux point. What mechanism can cause this saturation? Interestingly, both the dielectric and inductive loss can be readily eliminated by the parity selection rule [see Fig. 1(b)]. The saturation can be explained by indirect thermal processes, for example, an excitation $|2\rangle \to |3\rangle$, the estimated rate of which is indeed around 1 ms (using $\omega_{23}/2\pi = 1.66$ GHz and $T = 25$ mK), followed by a rapid direct relaxation $|3\rangle \to |0\rangle$ (Supplemental Material [18], note 7D). Theory also predicts a parity-violating direct decay, governed by the matrix element $\langle 2|\cos(\hat{\varphi}/2)|0\rangle \sim 1$, due to quasiparticle tunneling specifically across the weakest junction of fluxonium [35]. This mechanism includes photon-assisted tunneling (PAT) processes as well [36], altogether characterized by a dimensionless quasiparticle density x_{qp}, normalized by the density of Cooper pairs. Our observation that $T_1^{02} > 1.5$ ms translates into a direct upper bound $x_{qp} < 5 \times 10^{-9}$. For a transmon circuit, such as the one obtained from that in Fig. 1 by removing the inductive shunt and slightly adjusting the ratio of E_J/E_C, our bound on x_{qp} would be equivalent to $T_1 > 4$ ms.

The observation of $T_2^* > 1$ ms follows naturally from our previous work on fluxoniums [15]. There we measured devices with varying parameters and concluded that T_1 was limited by dielectric loss and T_2 was following T_1. In particular, for device I we observed $T_1 \sim T_2 \sim 500$ μs at the sweet-spot frequency of 395 MHz (T_2 was measured with a single π pulse echo). The present device has about twice

lower sweet-spot frequency, which reduces the dielectric loss rate for the same material quality. However, as we show in the present study, many factors can suppress the value of T_2^*, such as an unfortunate defect-induced fluctuation in the value of T_1, or residual photons in the readout cavity, or quasiparticle-induced relaxation or excitation processes. Much work is still required to built large-scale superconducting processors with millisecond-range coherence times, and our case study demonstrates the short-term feasibility of this goal.

We acknowledge the support from DOE-SC0019449 and the ARO-LPS HiPS Program (W911NF1810146).

[1] M. H. Devoret and R. J. Schoelkopf, Superconducting circuits for quantum information: An outlook, Science **339**, 1169 (2013).
[2] M. Kjaergaard, M. E. Schwartz, J. Braumüller, P. Krantz, J. I.-J. Wang, S. Gustavsson, and W. D. Oliver, Superconducting qubits: Current state of play, Annu. Rev. Condens. Matter Phys. **11**, 369 (2020).
[3] Y. Nakamura, Y. A. Pashkin, and J. S. Tsai, Coherent control of macroscopic quantum states in a single-Cooper-pair box, Nature (London) **398**, 786 (1999).
[4] D. Vion, A. Aassime, A. Cottet, P. Joyez, H. Pothier, C. Urbina, D. Esteve, and M. H. Devoret, Manipulating the quantum state of an electrical circuit, Science **296**, 886 (2002).
[5] H. Paik, D. I. Schuster, L. S. Bishop, G. Kirchmair, G. Catelani, A. P. Sears, B. R. Johnson, M. J. Reagor, L. Frunzio, L. I. Glazman, S. M. Girvin, M. H. Devoret, and R. J. Schoelkopf, Observation of High Coherence in Josephson Junction Qubits Measured in a Three-Dimensional Circuit QED Architecture, Phys. Rev. Lett. **107**, 240501 (2011).
[6] R. Barends, J. Kelly, A. Megrant, D. Sank, E. Jeffrey, Y. Chen, Y. Yin, B. Chiaro, J. Mutus, C. Neill, P. O'Malley, P. Roushan, J. Wenner, T. C. White, A. N. Cleland, and J. M. Martinis, Coherent Josephson Qubit Suitable for Scalable Quantum Integrated Circuits, Phys. Rev. Lett. **111**, 080502 (2013).
[7] F. Yan, S. Gustavsson, A. Kamal, J. Birenbaum, A. P. Sears, D. Hover, T. J. Gudmundsen, D. Rosenberg, G. Samach, S. Weber, J. L. Yoder, T. P. Orlando, J. Clarke, A. J. Kerman, and W. D. Oliver, The flux qubit revisited to enhance coherence and reproducibility, Nat. Commun. **7**, 12964 (2016).
[8] A. P. Place, L. V. Rodgers, P. Mundada, B. M. Smitham, M. Fitzpatrick, Z. Leng, A. Premkumar, J. Bryon, S. Sussman, G. Cheng, T. Madhavan, H. K. Babla, B. Jäck, A. Gyenis, N. Yao, R. J. Cava, N. P. de Leon, and A. A. Houck, New material platform for superconducting transmon qubits with coherence times exceeding 0.3 milliseconds, Nat. Commun. **12**, 1779 (2021).
[9] C. Rigetti, J. M. Gambetta, S. Poletto, B. L. T. Plourde, J. M. Chow, A. D. Córcoles, J. A. Smolin, S. T. Merkel, J. R. Rozen, G. A. Keefe, M. B. Rothwell, M. B. Ketchen, and M. Steffen, Superconducting qubit in a waveguide cavity with a coherence time approaching 0.1 ms, Phys. Rev. B **86**, 100506(R) (2012).
[10] F. Arute *et al.*, Quantum supremacy using a programmable superconducting processor, Nature (London) **574**, 505 (2019).
[11] P. Jurcevic *et al.*, Demonstration of quantum volume 64 on a superconducting quantum computing system, Quantum Sci. Technol. **6**, 025020 (2021).
[12] N. Ofek, A. Petrenko, R. Heeres, P. Reinhold, Z. Leghtas, B. Vlastakis, Y. Liu, L. Frunzio, S. M. Girvin, L. Jiang, M. Mirrahimi, M. H. Devoret, and R. J. Schoelkopf, Extending the lifetime of a quantum bit with error correction in superconducting circuits, Nature (London) **536**, 441 (2016).
[13] P. Campagne-Ibarcq, A. Eickbusch, S. Touzard, E. Zalys-Geller, N. E. Frattini, V. V. Sivak, P. Reinhold, S. Puri, S. Shankar, R. J. Schoelkopf, L. Frunzio, M. Mirrahimi, and M. H. Devoret, Quantum error correction of a qubit encoded in grid states of an oscillator, Nature (London) **584**, 368 (2020).
[14] V. E. Manucharyan, J. Koch, L. I. Glazman, and M. H. Devoret, Fluxonium: Single cooper-pair circuit free of charge offsets, Science **326**, 113 (2009).
[15] L. B. Nguyen, Y. H. Lin, A. Somoroff, R. Mencia, N. Grabon, and V. E. Manucharyan, High-Coherence Fluxonium Qubit, Phys. Rev. X **9**, 041041 (2019).
[16] Y.-H. Lin, L. B. Nguyen, N. Grabon, J. San Miguel, N. Pankratova, and V. E. Manucharyan, Demonstration of Protection of a Superconducting Qubit from Energy Decay, Phys. Rev. Lett. **120**, 150503 (2018).
[17] A. Blais, A. L. Grimsmo, S. M. Girvin, and A. Wallraff, Circuit quantum electrodynamics, Rev. Mod. Phys. **93**, 025005 (2021).
[18] See Supplemental Material at http://link.aps.org/supplemental/10.1103/PhysRevLett.130.267001 for additional information and supporting data on our experiments. We provide the theory for our analysis of the experimental results, and details of the cryogenic setup and device fabrication procedure.
[19] H. Zhang, S. Chakram, T. Roy, N. Earnest, Y. Lu, Z. Huang, D. K. Weiss, J. Koch, and D. I. Schuster, Universal Fast-Flux Control of a Coherent, Low-Frequency Qubit, Phys. Rev. X **11**, 011010 (2021).
[20] C. Wang, C. Axline, Y. Y. Gao, T. Brecht, Y. Chu, L. Frunzio, M. H. Devoret, and R. J. Schoelkopf, Surface participation and dielectric loss in superconducting qubits, Appl. Phys. Lett. **107**, 162601 (2015).
[21] K. N. Nesterov, I. V. Pechenezhskiy, C. Wang, V. E. Manucharyan, and M. G. Vavilov, Microwave-activated controlled- Z gate for fixed-frequency fluxonium qubits, Phys. Rev. A **98**, 030301(R) (2018).
[22] Q. Ficheux, L. B. Nguyen, A. Somoroff, H. Xiong, K. N. Nesterov, M. G. Vavilov, and V. E. Manucharyan, Fast Logic with Slow Qubits: Microwave-Activated Controlled-Z Gate on Low-Frequency Fluxoniums, Phys. Rev. X **11**, 021026 (2021).
[23] H. Xiong, Q. Ficheux, A. Somoroff, L. B. Nguyen, E. Dogan, D. Rosenstock, C. Wang, K. N. Nesterov, M. G. Vavilov, and V. E. Manucharyan, Arbitrary controlled-phase gate on fluxonium qubits using differential ac-Stark shifts, Phys. Rev. Res. **4**, 023040 (2022).

[24] P. V. Klimov *et al.*, Fluctuations of Energy-Relaxation Times in Superconducting Qubits, Phys. Rev. Lett. **121**, 090502 (2018).

[25] E. Magesan, J. M. Gambetta, and J. Emerson, Scalable and Robust Randomized Benchmarking of Quantum Processes, Phys. Rev. Lett. **106**, 180504 (2011).

[26] E. Magesan, J. M. Gambetta, B. R. Johnson, C. A. Ryan, J. M. Chow, S. T. Merkel, M. P. da Silva, G. A. Keefe, M. B. Rothwell, T. A. Ohki, M. B. Ketchen, and M. Steffen, Efficient Measurement of Quantum Gate Error by Interleaved Randomized Benchmarking, Phys. Rev. Lett. **109**, 080505 (2012).

[27] A. Bermudez, X. Xu, R. Nigmatullin, J. OGorman, V. Negnevitsky, P. Schindler, T. Monz, U. G. Poschinger, C. Hempel, J. Home, F. Schmidt-Kaler, M. Biercuk, R. Blatt, S. Benjamin, and M. Müller, Assessing the Progress of Trapped-Ion Processors Towards Fault-Tolerant Quantum Computation, Phys. Rev. X **7**, 041061 (2017).

[28] G. Feng, J. J. Wallman, B. Buonacorsi, F. H. Cho, D. K. Park, T. Xin, D. Lu, J. Baugh, and R. Laflamme, Estimating the Coherence of Noise in Quantum Control of a Solid-State Qubit, Phys. Rev. Lett. **117**, 260501 (2016).

[29] J. Wallman, C. Granade, R. Harper, and S. T. Flammia, Estimating the coherence of noise, New J. Phys. **17**, 113020 (2015).

[30] Z. Chen, Metrology of quantum control and measurement in superconducting qubits, Ph.D. thesis, 2018, https://web.physics.ucsb.edu/~martinisgroup/theses/Chen2018.

[31] J. H. Yeh, J. Lefebvre, S. Premaratne, F. C. Wellstood, and B. S. Palmer, Microwave attenuators for use with quantum devices below 100 mK, J. Appl. Phys. **121**, 224501 (2017).

[32] Z. Wang, S. Shankar, Z. K. Minev, P. Campagne-Ibarcq, A. Narla, and M. H. Devoret, Cavity Attenuators for Superconducting Qubits, Phys. Rev. Appl. **11**, 014031 (2019).

[33] F. Yan, D. Campbell, P. Krantz, M. Kjaergaard, D. Kim, J. L. Yoder, D. Hover, A. Sears, A. J. Kerman, T. P. Orlando, S. Gustavsson, and W. D. Oliver, Distinguishing Coherent and Thermal Photon Noise in a Circuit Quantum Electrodynamical System, Phys. Rev. Lett. **120**, 260504 (2018).

[34] I. M. Pop, K. Geerlings, G. Catelani, R. J. Schoelkopf, L. I. Glazman, and M. H. Devoret, Coherent suppression of electromagnetic dissipation due to superconducting quasiparticles, Nature (London) **508**, 369 (2014).

[35] L. I. Glazman and G. Catelani, Bogoliubov quasiparticles in superconducting qubits, SciPost Phys. Lect. Notes **31**, 16 (2021).

[36] M. Houzet, K. Serniak, G. Catelani, M. H. Devoret, and L. I. Glazman, Photon-Assisted Charge-Parity Jumps in a Superconducting Qubit, Phys. Rev. Lett. **123**, 107704 (2019).